Magnetic field calibration of a transmission electron microscope using a permanent magnet material

V. V. Volkov,[a] D. C. Crew, Y. Zhu, and L. H. Lewis
Materials Sciences Department, Brookhaven National Laboratory, Upton, New York 11973-5000

(Received 25 May 2001; accepted for publication 4 March 2002)

A new method of assessing the magnitude of the magnetic field in a transmission electron microscope using a permanent magnetic material is described. The approach is versatile and simple enough to be implemented for certain scientific or engineering situations in which the exact calibration of the magnetic field in the microscope column using a small Hall probe may be a problem. We have applied this approach to obtain the magnetic field calibration inside a JEM 3000F field emission electron microscope as a function of the objective lens potential. In the course of this *in situ* calibration it was not necessary to disassemble the microscope or interrupt its operation. The procedure used is versatile and accurate enough to measure magnetic fields up to 20 kOe ($\mu_0 H = 2$ T in SI units) as was confirmed by subsequent Hall-probe field measurement of the same electron microscope. The calibration method described in this article does not require any special Hall-probe holder adaptations and can be applied to any transmission electron microscope or similar instrument. To illustrate the utility of the technique and its results, quantitative analysis of magnetic domain images obtained with Lorentz microscopy during magnetic reversal of a sample subjected to an *in situ* magnetic field in the JEM3000F microscope is presented and discussed. © *2002 American Institute of Physics.* [DOI: 10.1063/1.1472465]

I. INTRODUCTION

The operation of a transmission electron microscope (TEM) requires that the sample of interest be placed within the objective lens (OL) magnetic pole pieces of the instrument. Thus during normal imaging operation the sample is subjected to an *in situ* magnetic field with a high value. Many transmission electron microscopes allow the OL to be switched off during the imaging procedure, a feature that is particularly useful for studies of magnetically sensitive samples using either the Fresnel or the Foucault imaging modes of the Lorentz microscopy technique. The presence of the OL does, however, provide a convenient way by which to vary the magnetic field surrounding the sample and to examine the effect of that field on the magnetic domain configuration of the sample. It is necessary that the application of a magnetic field to a magnetic sample during TEM imaging be done with care. Variation of the magnetic field applied to a sample within the TEM is usually achieved by varying the objective lens current, which may change the imaging conditions, or by varying the tilt of the specimen relative to the column axis, which changes the component of the OL magnetic field projected into the plane of a sample.

For quantitative magnetic TEM image analysis it is important to know the value of the magnetic field applied to a sample. Calibration of the magnetic field inside an electron microscope as a function of the OL current is not a simple procedure, because it usually requires the use of a special holder in conjunction with a Hall-effect probe. For example, the schematic cross-sectional layout of the JEM 3000F TEM column with a side-entry holder geometry presented in Fig. 1 illustrates that there is not enough room in the column to place additional magnetic field sensors close to the optical axis of the TEM column in the vicinity of the specimen area (Fig. 1, segment 7). Only a small part of the high-vacuum TEM column relevant to the specimen area and environment is shown here for clarity.[1] Hence, any independent magnetic field measurement can only be carried out with either a special TEM holder with a Hall probe or some other type of wireless magnetic sensor that must fit into the standard TEM specimen holder.

In this article we report a novel technique which avoids this complication by using the OL current to magnetize *in situ* an initially demagnetized but well-characterized magnetic specimen, henceforth referred to as a magnetic sensor, that acts as a probe of the magnetic field in the specimen area of the TEM. This technique bypasses the need for special and/or expensive Hall-effect probe attachments. As it is important to choose a magnetic sensor with a unique and reproducible magnetic field response, some brief magnetic materials selection criteria will be outlined. Details of the proposed field-calibration procedure of a TEM using such a magnetic sensor are described below. The results of this procedure are compared to those obtained by a conventional Hall-probe characterization of the magnetic field in the TEM. Finally, the utility of the technique is illustrated by quantitative analysis of Lorentz magnetic domain images obtained during the magnetic reversal of a sample subjected to an *in situ* magnetic field in the JEM 3000F microscope.

[a]Author to whom correspondence should be addressed; electronic mail: volkov@bnl.gov

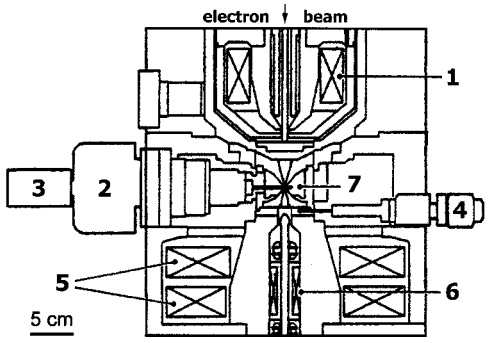

FIG. 1. Schematic cross-sectional layout of the TEM column in the specimen area. The following features are indicated: (1) condenser minilens (CM) coil; (2) goniometer; (3) specimen holder; (4) objective aperture assembly; (5) objective lens (OL) coils; (6) objective minilens (OM) coil; and (7) specimen area inside OL pole pieces.

II. PRINCIPLE OF CALIBRATION

A. Choice of sensor material

Calibration of the magnitude of the internal field inside the TEM is achieved by monitoring the development of remanent magnetization with OL potential during TEM imaging of a thermally demagnetized ferromagnetic sample of known magnetic response. In this endeavor it is necessary to utilize a permanent magnetic material which retains some fraction of magnetization achieved (the remanence M_r) after application and removal of an applied external field. The magnetic sensor chosen must not be magnetically saturated before the maximum field inside the TEM is reached. The technique and accuracy of the calibration are enhanced by the use of a magnetic sensor with an ideally linear magnetic response with field (i.e., a small magnetizing susceptibility) and without a multistage initial magnetization curve. It is also important that the magnetic material chosen does not exhibit thermal degradation in magnetic behavior, as it is necessary to thermally demagnetize the sensor multiple times to check the reproducibility of the technique. A magnetic material that satisfied the requirements outlined above is a hot-pressed fully dense nanocrystalline material based on the composition $Nd_2Fe_{14}B$ (Nd–Fe–B). The isotropic microstructure of this magnet, described elsewhere,[2] renders the magnetic properties suitable for use as a TEM magnetic sensor.

B. Experimental field calibration of the magnetic sensor

The material selected for the TEM magnetic sensor was a magnet made from melt-spun and subsequently hot-pressed $Nd_2Fe_{14}B$-based ribbons of nominal composition $Nd_{14}(Fe_{92}Co_8)_{80}B_6Ga_{0.5}$ obtained from General Motors Research Laboratories in Warren, Michigan. The processing details of the magnet are discussed elsewhere.[3–5] A uniform disk of 3 mm in diameter was cut from the center of the sample and polished to a final thickness of 0.15 mm by hand with 800 grit (10 μm) silicon carbide paper. These dimensions represent the maximum dimensions that can fit into a standard TEM sample holder.

The polished Nd–Fe–B disk was sealed in a quartz tube in a vacuum of approximately 3×10^{-6} Torr and heated briefly to 400 K, above the Curie temperature of $Nd_2Fe_{14}B$, to thermally demagnetize the sample. Upon cooling this procedure creates a distribution of magnetic domains with a random magnetization orientation and thus allows the magnetic remanent state to be set to zero. The demagnetized sample was then inserted into a Quantum Design MPMS superconducting quantum interference device (SQUID) magnetometer with the normal to the disk surface aligned with the applied field direction. It was important to maintain this measurement geometry because it mimicked the geometry of the sample within the TEM. The sample was magnetized at $T=300$ K by stepping the applied magnetic field in increments and then reducing the field back to zero, thus recording the remanence associated with each increase in applied field. This procedure was repeated to a maximum applied field of 50 kOe. Partial magnetization loops, known as recoil loops, are obtained by this procedure and are shown in Fig. 2. It should be noted that the partial recoil loops are entirely reversible, indicating little contribution of irreversible processes to the magnetization and subsequent demagnetization processes. The *ex situ* field-calibration curve (Fig. 3) was reproducible to within about 4% after multiple cycles of magnetization and thermal demagnetization. The error in reproducibility is most likely associated with sample mounting irregularities rather than intrinsic material variation and is discussed in the error analysis in Sec. IV. The reproducibility of the partial demagnetization curves defines a one-to-one relationship between the remanence of the magnetic material and the applied field. It also displays an almost linear remanence response versus applied field up to 20 kOe, with a demonstrated flattening towards magnetic saturation above this field.

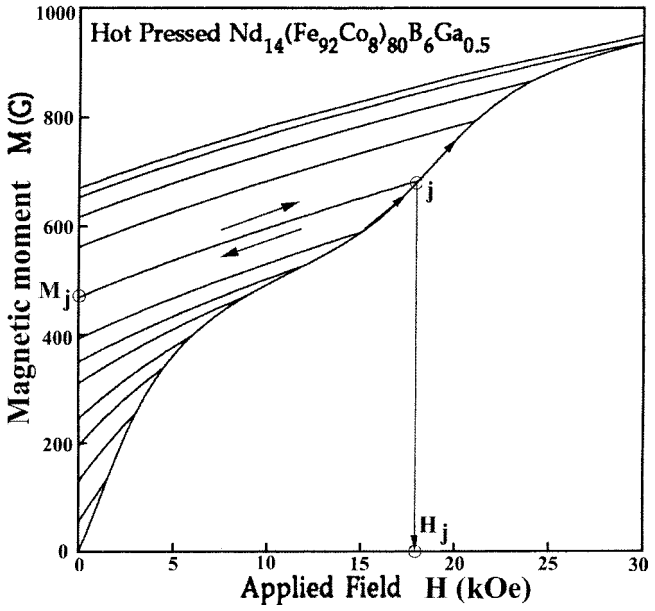

FIG. 2. Magnetic recoil curves used to determine magnetic remanence of the magnetic sensor sample $Nd_{14}(Fe_{92}Co_8)_{80}B_6Ga_{0.5}$ measured at room temperature with the SQUID magnetometer. This set of measurements establishes an unambiguous relationship between the remanence (M_r) of the magnetic sensor and the magnitude of the applied magnetic field (H).

This procedure constitutes the general principle used in this work for the calibration of the magnetic field produced

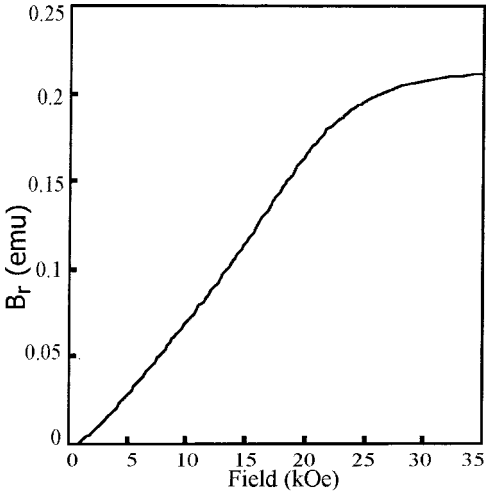

FIG. 3. Remanent magnetization response of the magnetic sensor sample as a function of applied magnetic field measured by the SQUID magnetometer at room temperature and obtained from the partial magnetic recoil curves in Fig. 2.

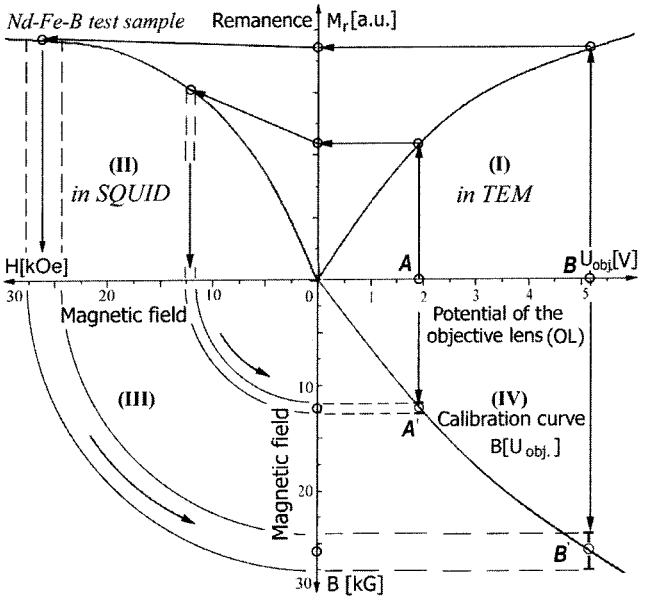

FIG. 4. Schematic of the principle underlying the magnetic field calibration method using a magnetic sensor. Quadrant I is the sensor magnetization response vs the OL potential as a function of the magnetic field in the electron microscope to be determined. Quadrant II is sensor response to the known magnetic field generated in the SQUID magnetometer. Quadrants III and IV show the construction of the final calibration curve of TEM magnetic field B vs OL potential U_{obj}. Points A and B indicate that at higher magnetic fields the experimental errors are expected to be more significant due to magnetic saturation of the sensor.

by the objective lens in the sample area of a JEM 3000F field emission electron microscope operating at accelerating voltages of 200–300 kV.

III. EXPERIMENTAL FIELD CALIBRATION OF THE TEM

A. Field calibration using a magnetic sensor

Magnetic field determination inside the JEM 3000F TEM was accomplished in two independent ways: using the measured magnetic response of the magnetic sensor previously calibrated and, later, using a Hall probe. A significant advantage of the former method is that it does not require the use of any special TEM holder with a Hall-probe unit. The field calibration performed with the magnetic sensor is versatile enough to be applied to the field calibration of any TEM or another similar machine. After completion of the *ex situ* magnetic remanence calibration, the magnetic sensor was once more sealed in an evacuated quartz tube and then thermally demagnetized at 400 K. The demagnetized magnetic sensor was then placed in the specimen holder and inserted into the TEM. The sensor was gradually magnetized in the TEM column in increments by increasing the OL potential. For the transmission electron microscope utilized in this study the OL potential U_{obj} is related to the objective lens current I_{obj} by the relation $U_{obj}=I_{obj}R_{obj}$, where $R_{obj}=0.372\,\Omega$ is a reference resistance in the OL-coil circuit. After each cycle of increase and decrease in OL potential U_{obj} in the TEM the magnetic sensor was removed and its remanence was measured in zero field with the SQUID magnetometer. This procedure was repeated several times for progressively larger values of objective lens current in the TEM, and is shown schematically in Fig. 4. Special care was taken to ensure that the test sample had the same position and orientation with respect to the field both in the TEM and in the SQUID magnetometer.

Figure 4 is a schematic representation of the relationship between the magnetization response of the magnetic sensor versus applied magnetic field both in the TEM and in the SQUID magnetometer that is used to provide a calibration curve. The first quadrant of the diagram in Fig. 4, labeled (I), represents the transfer function of the magnetic sensor magnetization response $M_r(U_{obj})$ versus the unknown magnetic field $H(U_{obj})$ produced by the TEM OL coil potential U_{obj}. The second quadrant of the diagram, labeled (II), displays the transfer function of the magnetic sensor remanent magnetization $M_r(H)$ as a function of the magnetic field applied in the SQUID magnetometer. This is simply a schematic plot of the *ex situ* magnetic recoil curves of the magnetic sensor originally shown in Fig. 2. The $(-Y)$ and $(-X)$ axes in Fig. 4 are identical and are used to construct the final value of magnetic field H generated in the microscope ($-Y$ axis) versus the OL potential U_{obj} (X axis). Quadrant IV contains the final calibration curve of the field $B(U_{obj})$ generated in the TEM as a function of the OL potential. Here we assume $B(U_{obj})=H(U_{obj})$ because B is numerically equal to H for the ''air gap'' of OL pole pieces of the TEM, since the permeability of vacuum $\mu_{vac}=B_{vac}/H=1$ in centimeter–gram–second (cgs) units. The advantage of this field-calibration method is that the final result should not be sensitive to the specific shape of the experimental calibration curve $M_r(H)$ for the magnetic sensor used (Fig. 3). Details concerning the error induced by the test-sample method are provided in Sec. IV.

Depending upon the specific material, the effects of magnetic saturation at high fields of the magnetic sensor sample (Fig. 3) on the calibration curve $M_r(H)$ may be a source of significant experimental error for the TEM field-calibration curve $H(U_{obj})$. As one can see in Fig. 5 the am-

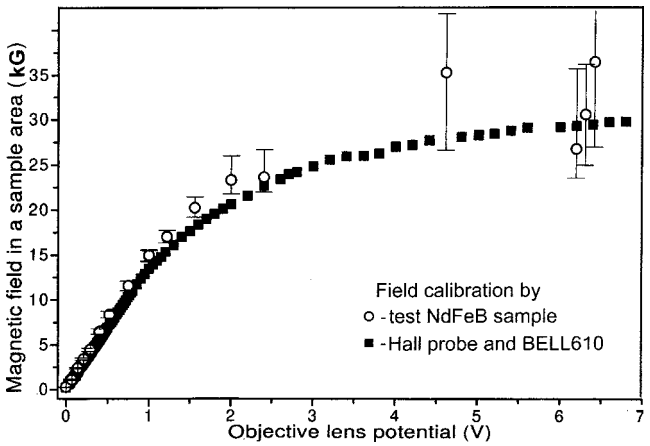

FIG. 5. Final calibration curve of the magnetic field in the specimen area of the JEM 3000F microscope as a function of the OL potential measured by two independent methods: (a) the Nd–Fe–B magnetic test sensor method (open circles) and (b) the Hall-probe method (closed squares). The calibration curve (b) is universal for all TEM modes of microscope listed in Table I and defined by the TEM's computer.

plitude of the experimental error in remanent magnetization increases for $H \geqslant 20$ kOe as the magnetic sensor approaches saturation magnetization. A discussion of the inherent error in the TEM field determination is facilitated by a close examination of Fig. 4 where point A′ represents the low-field region of the TEM field-calibration curve and point B′ represents the high-field region of the calibration curve. The experimental error in the field determined for point B′ in Fig. 4 (quadrant IV) is noticeably larger than that of point A′ (quadrant IV), as quantified by the parallel dashed lines. This difference in experimental error is attributed to the lower sensitivity of the sensor magnetization response to applied field as it approaches the high-field limit. In general, the accuracy of the technique decreases as the susceptibility of the sample decreases at high fields.

In situ Lorentz imaging is only possible at magnetic fields below a certain maximum applied field that is specific to the magnetic material under investigation. For instance, the *in situ* magnetic imaging of the magnetic domain structure in Nd–Fe–B-based permanent magnets is not possible above fields of $H_{max} > 15$ kOe, because the magnet is saturated at $H_{sat} \sim 20$ kOe (see Fig. 3) and the domain structure disappears. Additionally, a very strong demagnetizing field that surrounds the saturated sample may alter the parallel electron beam passing through sample and spoil the sensitivity of the magnetic image as well. It is fortunate therefore that the decrease in calibration accuracy produced by the magnetic saturation of the Nd–Fe–B sample using this technique does not affect the low-field calibration.[6]

B. Field calibration using a Hall probe

The *in situ* magnetic field calibration in the sample area of an electron microscope using a permanent magnetic material as a magnetic sensor, outlined above, was successfully verified by a subsequent independent magnetic field calibration of the same JEM 3000F instrument using a special TEM specimen holder containing a Hall probe. This procedure only became possible during disassembly and maintenance of the microscope. During this procedure a special tilt goniometer unit (Fig. 1, items 2 and 3) was removed to allow direct access to the OL pole pieces through the flange window (Fig. 1, item 7). A long holder with a small Hall probe mounted on the tip was used for direct field measurement of the magnetic field in the TEM OL pole–piece gap. The results of these independent field measurements are also shown as closed squares in Fig. 5 and are summarized in Table I. The Hall probe itself was calibrated in a well-calibrated static magnetic field generated by a variable Nd–Fe–B magnet[7,8] and was found to exhibit a linear response with the field, offset by 5 G at zero applied field. It is clear that this second calibration curve $B(U_{obj})$ obtained by the Hall probe (Fig. 5) has a smaller experimental error, as is shown in the low-field limit region in Fig. 6.

More experimental results of the magnetic field of the JEM 3000F microscope as a function of different operating conditions and magnifications are presented in Table I. Notice that the random error in the field measured by the Hall

TABLE I. Magnetic field in specimen area of the JEM 3000F microscope under various operating conditions.

Accelerating voltage = 200 kV			Accelerating voltage = 300 kV		
	U_{obj} (V)[a]	Field B (kG)[b]		U_{obj} (V)[a]	Field B (kG)[b]
Low magnification			Low magnification		
60×–1500×	0.06	0.985	60×–1500×	0.07	1.121
2000×–3000×	0.01	0.172	2000×–3000×	0.01	0.172
Holography low magnification[c]			Holography low magnification		
2000×–4000×	0.01	0.172	2000×–4000×	0.27	3.785
Magnification			Magnification		
4000×–6000×	4.32	27.654	4000×–6000×	6.28	29.622
8000×–150 0000×	4.32	27.654	8000×–150 0000×	6.30	29.637

[a]The OL potential U_{obj} is related to OL current I_{obj} by the relation $U_{obj} = I_{obj} * R_{obj}$, where $R_{obj} = 0.372\ \Omega$ is a reference resistance in the OL coil circuit.
[b]The experimental data of magnetic field B (kG) vs U_{obj} (V) were recorded by a Hall probe with accuracy ±15 G, if not specified in the text.
[c]Special TEM mode used for the electron holography applications.

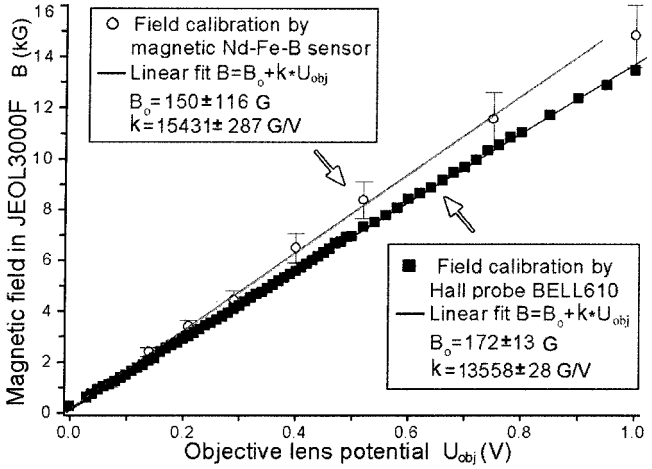

FIG. 6. Low-field part of the calibration curve found to be suitable for *in situ* magnetic imaging of the domain structure of Nd–Fe–B magnets. The open circles represent the result obtained by the Nd–Fe–B magnetic sensor. The closed squares indicate the independent calibration curve obtained by the Hall probe equipped with a BELL610 gaussmeter. For the latter the accuracy of the Hall probe was verified by a calibrated variable field magnet in the Multimag MM2000-26.5 apparatus (Refs. 7 and 8). The errors marked with ± were obtained by linear extrapolation of the experimental data towards zero field.

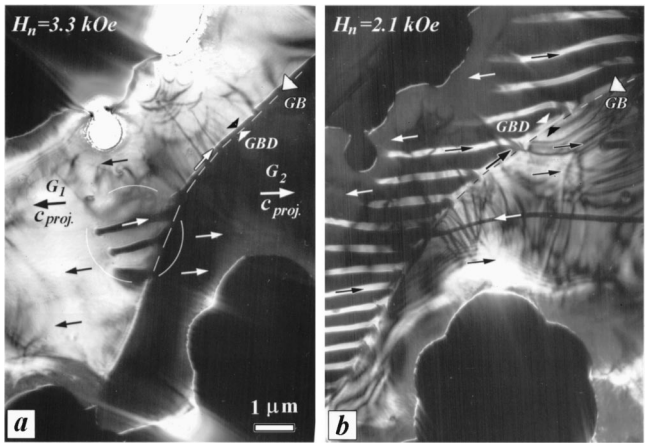

FIG. 7. Magnetic images of the grain boundary area in a sintered Nd–Fe–B magnet recorded in Foucault mode vs decreasing applied magnetic fields of 3.3 (a) and 2.1 kOe (b). Details of the two images are provided in the text. Nucleation and expansion of reverse magnetic domains in grain G_1 (a) can be seen to occur via formation of a small domain at the grain boundary. The dashed line indicates the grain boundary, and the fine arrows show the local in-plane directions of domain magnetization. The projected in-plane magnetization directions are opposite for grains G_1 and G_2, as is evident from their black/white Foucault contrast. Diffraction analysis confirmed that grains G_1 and G_2 have parallel in-plane components of the *c* axes projected into the plane of the image; these *c* axes enclose a dihedral angle of about 84°.

probe did not exceed ±15 G. Other important experimental parameters of the magnetic field-calibration procedures described above are as follows.

Figure 5 indicates that the experimentally determined magnetic field generated by the OL in the specimen area of the JEM 3000F microscope in ordinary TEM mode is around 25 kG (electron gun accelerating voltage=200 kV) or 30 kG (electron gun accelerating voltage=300 kV), as listed in Table I. The magnetic remanence of the OL pole pieces, measured after the application and removal of the maximum OL current, produces a residual magnetic field equal to 150 ±100 G (determined by the magnetic sensor method) or to 172±13 G (determined by the Hall-probe method, Fig. 6). These values are obtained from extrapolations of the magnetic data obtained by the two methods in Fig. 6 to zero field. These results appear to be consistent with one another and the remanent field in the microscope at zero OL current should be in the range of 150–170 G. This field is the minimum one present in the microscope regardless of the imaging mode used. The presence of a remanent field in the microscope also warrants special care be taken during quantitative magnetic analysis of magnets with coercivities below 200 Oe. Finally, as follows from Figs. 5 and 6, the linear part of field dependence $B(U_{\mathrm{obj}})$ extends up to a field of $B<15$ kG [1.5 T in Systeme International (SI) units] with $U^{s}_{\mathrm{obj}} \leqslant 1.0$ V (Fig. 6). To good approximation this part of the curve can be expressed by a simple linear formula on the basis of Hall-probe data (Fig. 6) as

$$B\ (\mathrm{G}) = (172 \pm 13) + (133\,56 \pm 28) * U_{\mathrm{obj}}, \qquad (1)$$

where B is the magnetic field in the specimen area of TEM measured in gauss and U_{obj} is the OL potential measured in volts. The constant 133 56 in Eq. (1), in units of G/V, quantifies the sensitivity of the magnetic field to the OL potential. Notice that the sensitivity determined by the magnetic sensor calibration method is a little higher than that measured by the Hall probe; this issue will be explored in Sec. IV. Figures 5 and 6 demonstrate that both of the calibration methods used in the present work, within their respective experimental errors, appear to be consistent, resulting in almost the same calibration curves for the magnetic field generated by variation of the OL potential.

C. Application of results to quantitative magnetic imaging

Precise knowledge of the magnetic field excited in the specimen area of an electron microscope as a function of the OL potential allows one to take qualitative imaging of magnetic domain behavior obtained in Lorentz and/or Foucault modes[9,10] to a new quantitative level. The in-plane component of the projected magnetic field is defined by the expression $H_{\perp} = H \sin \alpha$, where α is the tilt angle of a sample plane in the goniometer (for the JEM 3000F microscope $|\alpha| < 26°$), where H is the field exited by the objective lens. With knowledge of the applied field, detailed analyses of TEM magnetic images recorded under *in situ* magnetizing conditions at the nanoscale become a reality. This approach may be fruitful for a quantitative description of the evolution of the local domain structure versus the applied field as well as enable the evaluation of magnetization and demagnetization processes, allowing one to differentiate between domain wall nucleation and domain wall pinning mechanisms that are sensitive to the sample composition, defect state, and applied magnetic field.

As an example of the utility of the approach, it is possible to elucidate the demagnetization process, shown in Fig. 7, by magnetic sensitive in-focus Foucault images, which depict the magnetic domain configuration present in a large-

angle grain boundary (GB) region in a sintered Nd–Fe–B magnet obtained by appropriate shift of the objective aperture. Under ''free lens control'' in the TEM the sample was magnetized first with field $H_n = 11$ kOe (Fig. 5) applied along the normal to the image plane. The experimental images were recorded after reducing field H_n, normal to the image plane, down to 3.3 and 2.1 kOe, respectively. The region imaged contains two grains, G_1 and G_2, approximately 5 μm in diameter with the different crystallographic orientations labeled; the dashed white line (labeled ''GB'') indicates the grain boundary. The black-and-white stripe contrast in Fig. 7 is magnetic domain contrast that arises from in-plane magnetization components with opposite orientations. The projected magnetization directions are opposite for grains G_1 and G_2, as is evident from their black/white Foucault contrast. Small arrows signify the in-plane magnetization direction of the grains. A small region that runs along the grain boundary, labeled ''GBD,'' indicates the presence of a grain boundary magnetic domain. The position of the grain boundary in the image was determined by removal of the objective aperture from the optical axis of the TEM. It is hypothesized that the presence of the grain boundary domain may reduce the magnetostatic energy in the intergranular area. The black regions in the upper-left corner and in the lower-right corner mark holes in the film. A small region of reverse magnetization (circled) is visible in grain G_1 near the grain boundary. Upon reduction of the objective lens current, and hence reduction of the magnetic field in a sample area, Fig. 7(b) shows that the reverse magnetization nucleus of grain G_1 has expanded and encompasses the entire grain. It is deduced that nucleation and expansion of reverse magnetic domains that exist in grain G_1 occur via the formation of the grain boundary domain (GBD). *In situ* TEM observation of the demagnetization process of this region indicates that the domain configuration changes abruptly with a reduction of the magnetic field from 3.3 to 2.1 kG.

A selected area electron diffraction analysis confirmed that the *c* axes of grains G_1 and G_2 span an angle of 84° and that the in-plane components of the *c* axes appear to be parallel when projected onto the image plane. This result is consistent with the magnetic anisotropy easy axis in $Nd_2Fe_{14}B$, which lies parallel to the *c* axis.[5] With knowledge of the applied magnetic field magnitude it is possible to separate the demagnetization process into three successive steps. The first step is a combined nucleation and expansion of the narrow GBD.[11] In the geometry imaged within the TEM foil this step occurs at nucleation field of $H_n = 3.3$ kOe. It appears that this specific grain boundary domain does not follow the easy magnetic axis of the grains, but instead, follows the grain boundary interface. The second step in the demagnetization process is the passage of the domain wall from the defective region into the grain interior.[11] This result is shown in Fig. 7(b) and occurs at a propagation field of $H_p = 2.1$ kOe. Further decreases in the applied field combined with the complex stray field cause the observed domain structure to evolve by expansion of the domain walls via additional lateral movement (not shown in Fig. 7). This is the last step in the local demagnetization process in this sintered Nd–Fe–B magnet.

IV. DISCUSSION OF SOURCES OF ERROR IN THE CALIBRATION

The goal of this exercise was to ascertain the magnetic field value produced by the objective lens current (or its potential) in the sample region of the TEM. Logically there is an unambiguous functional relationship between these two parameters. Experimentally it was found that only the OL contributes to the excited magnetic field in the specimen area of the JEM 3000F microscope. Hall probe measurements confirm that the other lenses in the microscope, such as the condenser minilens (CM) or the objective minilens (OM) shown in Fig. 1, do not contribute to the magnetic field in the specimen area and therefore their effects were neglected. Figures 5 and 6, however, indicate the existence of a certain average discrepancy in the field value obtained by the two measuring methods. In particular, the measured magnetic field in the TEM using the magnetic sensor method appears to be slightly higher (by a factor of 1.13) than the field obtained by the Hall-probe method for the same OL potential setting (Fig. 6). Two categories of experimental error have been considered to explain this discrepancy: random or statistical error and systematic error. It was concluded that one source of error results from the SQUID magnetometer remanent moment determination of the sensor sample. From experience with the SQUID magnetometer the random experimental error in the moment determination for a particular sample is approximately $\pm 0.5\%$, which represents the accuracy of the SQUID magnetometer and its associated electronics. However, a larger systematic error (on the order of $\sim 5\%$) can occur from inconsistent axial alignment of the sample with respect to the applied magnetic field axis in the SQUID. The error bars shown in Fig. 5 were calculated with the inclusion of the random error in the remanence M_r determination of 0.5%, and a variation in the placement of the sample, specifically in the angle of the sample normal with respect to applied field in the SQUID (5%). Taken together, these produce an error of not more than 5.5%. These error bars obviously represent unlikely extreme cases of systematic and random errors combined.

Another source of systematic error can be derived from the more accurate analysis performed for the OL magnetic circuit of the TEM. By applying Ampere's law $\oint Hdl = NI$ (where *NI* is a number of A/turns) to the closed magnetic circuit of the objective lens it is easy to show that the placement of a magnetic material inside the air gap of an electromagnet should increase its strength and hence the magnetic field inside the pole pieces. Our test sample was of finite thickness $h = 0.15$ mm, compatible with the air-gap width of the OL pole pieces ($l = 2$ mm) of the JEM 3000F microscope. A simplified calculation[12] of the magnetomotive force necessary to overcome the air-gap resistance of the OL lens allows an estimation of the magnetic field enhancement in the air gap:

$$B\ (\text{test sample})/B\ (\text{Hall probe}) = 1 + \frac{h}{l}\left(\frac{\mu - 1}{\mu}\right) \approx 1 + \frac{h}{l} = 1 + \frac{0.15}{2} \approx 1.08, \quad (2)$$

where $h = 0.15$ mm is the thickness of the specimen and l

$=2$ mm is the air-gap width of the OL pole pieces of the JEM 3000F microscope. This expression provides an estimate of the additional magnetic field in the OL gap induced by the magnetic sensor.

Taken together, the sources of systematic error mentioned above ($1.05 \cdot 1.08 = 1.13$ or a 13% difference) are sufficient to account for differences in the results obtained by the two different methods to evaluate the magnetic field present in the TEM. Under the reasonable assumption that the Hall probe provided a more accurate determination of the magnetic field within the TEM sample area, it is apparent that a small scaling factor correction of at least $\approx 8\%$ by Eq. (2) to the data derived from the magnetic sensor should be applied to the experimental data obtained with the magnetic sensor. However, the method-induced differences in the determination of the magnetic field as a function of the OL potential are small enough and therefore can be neglected in the typical range of magnetic fields (less than 15 kG) utilized for Lorentz and Foucault magnetic imaging. The accuracy of the Nd–Fe–B magnetic sensor field-calibration technique is sufficient to be used at fields below ~ 20 kOe. Above this value of the field the reduction in the magnetic susceptibility of the sensor as magnetic saturation is approached, as indicated by the calibration curves of Figs. 2 and 3, causes the accuracy of the technique to be compromised. With knowledge of the magnetic field in the TEM, a detailed analysis of *in situ* TEM magnetic domain images and other magnetic phenomena at the nanoscale becomes a reality.

ACKNOWLEDGMENT

This research was supported by the U.S. Department of Energy, Division of Materials, Office of Basic Energy Science, under Contract No. DE-AC02-98CH10886. The authors gratefully acknowledge Dr. Carl Fuerst of General Motors Research Laboratories for providing them with the magnetic sample.

[1] Manual for JEM-3000F field emission electron microscope; Part 3: Composition and Construction; Fig. 3.3-2, pp. 3–4, JEOL USA, Inc., 11 Dearborn Rd, Peabody, MA 01960.
[2] R. K. Mishra, J. Appl. Phys. **62**, 967 (1987); E. Burzo, Rep. Prog. Phys. **61**, 1099 (1998).
[3] C. D. Fuerst and E. G. Brewer, J. Appl. Phys. **73**, 5751 (1993).
[4] L. H. Lewis, T. R. Thurston, V. Panchanathan, U. Wildgruber, and D. O. Welch, J. Appl. Phys. **82**, 3430 (1997).
[5] J. F. Herbst, Rev. Mod. Phys. **63**, 819 (1991).
[6] V. V. Volkov, D. C. Crew, Y. Zhu, and L. H. Lewis, Microanal. **5** (Suppl. 2), 46 (1999).
[7] Variable magnet ''Multimag'' MM2000-26.5 manufactured by Magnetic Solutions Ltd., 1998, Lake Shore Cryotronics Inc., 575 McCorkie Boulevard, Westterville, OH 43082 (http://www.magnetic-solutions.com/).
[8] T. R. Ni Mhiochain, D. Weaire, S. M. McMurry, and J. M. D. Coey, J. Appl. Phys. **86**, 6412 (1999); M. G. Abele and H. A. Leupold, *ibid.* **64**, 5988 (1988).
[9] P. Hirsch, A. Howie, R. B. Nicholson, D. W. Pashley, and M. J. Whelan, *Electron Microscopy of Thin Crystals*, 2nd ed. (Krieger, Huntington, NY, 1977), p. 388.
[10] Y. Zhu and V. V. Volkov, in *Experimental Methods in the Physical Science*, edited by M. De Graef and Y. Zhu (Academic, New York, 2001) Vol. 36, Chap. 8, p. 227.
[11] D. Givord and M. F. Rossignol, in *Rare-Earth Iron Permanent Magnets*, edited by J. M. D. Coey (Clarendon, Oxford, 1996), Chap. 5, p. 218.
[12] S. Chikazumi, *Physics of Magnetism* (Krieger, Malabar, FL, 1964), p. 554.